OPTIMIZATION OF A HIGH EFFICIENCY FREE ELECTRON LASER AMPLIFIER

E.A. Schneidmiller, M.V. Yurkov, DESY, Hamburg, Germany

Abstract

Technique of undulator tapering in the post-saturation regime is used at the existing X-ray FELs for increasing the radiation power. We present comprehensive analysis of the problem in the framework of one-dimensional and three-dimensional theory. We find that diffraction effects essentially influence on the choice of the tapering strategy. Our studies resulted in a general law of the undulator tapering for a seeded FEL amplifier as well as for SASE FEL.

INTRODUCTION

Effective energy exchange between the electron beam moving in an undulator and electromagnetic wave happens when resonance condition takes place. In this case electromagnetic wave advances electron beam by one radiation wavelength while electron beam passes one undulator period. When amplification process enters nonlinear stage, the energy losses by electrons become to be pronouncing which leads to the violation of the resonance condition and to the saturation of the amplification process. Application of the undulator tapering [1] allows to a further increase of the conversion efficiency. An idea is to adjust undulator parameters (field or period) according to the electron energy loss such that the resonance condition is preserved.

It is generally accepted that in the framework of the one-dimensional theory an optimum law of the undulator tapering should be quadratic [2–9]. Similar physical situation occurs in the FEL amplifier with a waveguide [2]. In this case radiation is confined within the waveguide. Parameters of FEL amplifiers operating in the infrared, visible, and x-ray wavelength ranges are such that these devices are described in the framework of three dimensional theory with an "open" electron beam, i.e. physical case of diffraction in a free space. In this case the diffraction of radiation is an essential physical effect influencing optimization of the tapering process. Discussions and studies on the optimum law of the undulator tapering in the three-dimensional case are in the progress for more than 20 years. Our previous studies were mainly driven by occasional calculations of perspective FEL systems for high power scientific (for instance, FEL based $\gamma\gamma$ - collider) and industrial applications (for instance, for isotope separation, and lithography [10–12]). Their parameter range corresponded to the limit of thin electron beam (small value of the diffraction parameter). In this case linear undulator tapering works well from almost the very beginning [6]. Comprehensive study devoted to the global optimization of tapered FEL amplifier with "open" electron beam has been presented in [4]. It has been shown that: i) tapering law should be linear for the case of thin electron beam, ii) optimum tapering at the initial stage should follow quadratic dependence, iii) tapering should start approximately two field gain length before saturation. New wave of interest to the undulator tapering came with the development of x-ray free electron lasers [13–20]. Undulator tapering has been successfully demonstrated at long wavelength FEL amplifiers [2, 21], and is routinely used at x-ray FEL facilities LCLS and SACLA [16, 17]. Practical calculations of specific systems yielded in several empirical laws using different polynomial dependencies (see [22, 23] and references therein).

Comprehensive analysis of the problem of the undulator tapering in the presence of diffraction effects has been performed in [24,25]. It has been shown that the key element for understanding the physics of the undulator tapering is given by the model of the modulated electron beam which provides relevant interdependence of the problem parameters. Finally, application of similarity techniques to the results of numerical simulations led to the universal law of the undulator tapering. In this paper we extend studies [24, 25] to the case of SASE FEL.

BASIC RELATIONS

We consider axisymmetric model of the electron beam. It is assumed that transverse distribution function of the electron beam is Gaussian, so rms transverse size of matched beam is $\sigma = \sqrt{\epsilon\beta}$, where ϵ is rms beam emittance and β is focusing beta-function. An important feature of the parameter space of short wavelength FELs is that the space charge field does not influence significantly the amplification process, and in the framework of the three-dimensional theory the operation of the FEL amplifier is described by the following parameters: the diffraction parameter B, the energy spread parameter $\hat{\Lambda}_T^2$, the betatron motion parameter $\hat{k}_\beta$ and detuning parameter $\hat{C}$ [9, 26]:

$$B = 2\Gamma\sigma^2\omega/c\,, \qquad \hat{C} = C/\Gamma\,,$$
$$\hat{k}_\beta = 1/(\beta\Gamma)\,, \qquad \hat{\Lambda}_T^2 = (\sigma_E/\mathcal{E})^2/\rho^2\,, \qquad (1)$$

where $\Gamma = \left[I\omega^2\theta_s^2 A_{JJ}^2/(I_A c^2\gamma_z^2\gamma)\right]^{1/2}$ is the gain parameter, $\rho = c\gamma_z^2\Gamma/\omega$ is the efficiency parameter, and $C = 2\pi/\lambda_w - \omega/(2c\gamma_z^2)$ is the detuning of the electron with the nominal energy $\mathcal{E}_0$. Note that the efficiency parameter ρ entering equations of three dimensional theory relates to the one-dimensional parameter ρ_{1D} as $\rho_{1D} = \rho/B^{1/3}$ [9, 27]. The following notations are used here: I is the beam current, $\omega = 2\pi c/\lambda$ is the frequency of the electromagnetic wave, $\theta_s = K/\gamma$, K is the rms undulator parameter, $\gamma_z^{-2} = \gamma^{-2} + \theta_s^2$, $k_w = 2\pi/\lambda_w$ is the undulator wavenumber, $I_A = 17$ kA is the Alfven current, $A_{JJ} = 1$ for helical undulator and $A_{JJ} = J_0(K^2/2(1+K^2)) - J_1(K^2/2(1+K^2))$ for planar undulator. J_0 and J_1 are the Bessel functions of the first

ISBN 978-3-95450-134-2

Copyright © 2015 CC-BY-3.0 and by the respective authors

kind. The energy spread is assumed to be Gaussian with rms deviation σ_E.

In the following we consider the case of negligibly small values of the betatron motion parameter $\hat{k}_\beta$ and the energy spread parameter $\hat{\Lambda}_T^2$ (i.e. the case of "cold" electron beam). Under these assumptions the operation of the FEL amplifier is described by the diffraction parameter B and the detuning parameter $\hat{C}$.

Equations, describing the motion of the particles in the ponderomotive potential well of the electromagnetic wave and the undulator, become simple when written down in the normalized form (see, e.g. [9]):

$$\frac{d\Psi}{d\hat{z}} = \hat{C} + \hat{P}, \qquad \frac{d\hat{P}}{d\hat{z}} = U\cos(\phi_U + \Psi)\,, \qquad (2)$$

where $\hat{P} = (E - E_0)/(\rho E_0)$, $\hat{z} = \Gamma z$, and U and ϕ_U are the amplitude and the phase of the effective potential. Deviation of the electron energy is small in the exponential stage of amplification, $\hat{P} \ll 1$, and process of the beam bunching in phase Ψ lasts for a long distance, $\hat{z} \gg 1$. Situation changes drastically when amplification process enters nonlinear stage and deviation of the electron energy $\hat{P}$ approaches to the unity. The phase change on a scale of $\Delta\hat{z} \simeq 1$ becomes to be fast, particles start to slip fast in phase Ψ which leads to the reduction of the electron beam modulation, and the growth of the radiation power is saturated.

Undulator tapering [1], i.e. adjustment of the detuning according to the energy loss of electrons, $\hat{C}(\hat{z}) = -\hat{P}(\hat{z})$, allows to keep synchronism of trapped electrons with electromagnetic wave.

UNIVERSAL TAPERING LAW

During amplification process the electron beam is modulated periodically at the resonance wavelength. This modulation grows exponentially in the high gain linear regime, and reaches a value about the unity near the saturation point. Application of the undulator tapering allows to preserve beam bunching at a long distance. Electron beam current $I(z,t) = I_0[1 + a_{\rm in}\cos\omega(z/v_z - t)]$ is modulated with amplitude $a_{\rm in}$ in this case. Radiation power of the modulated beam is given by [28]:

$$\begin{aligned} W &= \frac{2\pi^2 I_0^2 a_{\rm in}^2 \sigma^2}{c\lambda\lambda_{\rm u}} \frac{K^2 A_{\rm JJ}^2}{1+K^2} f(\tilde{z})\tilde{z}\,, \\ f(\tilde{z}) &= \arctan(\tilde{z}/2) + \tilde{z}^{-1}\ln\left(\frac{4}{\tilde{z}^2+4}\right)\,. \end{aligned} \qquad (3)$$

In the right-hand side of expression (3) we explicitly isolated z-dependence of the radiation power with function $f(\tilde{z})$ of argument $\tilde{z} = 1/N$ where $N = k\sigma^2/z$ is Fresnel number, and $k = 2\pi/\lambda$ is wavenumber. Plot of the function $f(\tilde{z})$ is shown in Fig. 1. Asymptotes of the function $f(\tilde{z})$ are:

$$\begin{aligned} f(\tilde{z}) &\to \pi/2 \quad \text{for} \quad \tilde{z} \gg 1 \quad (N \ll 1)\,, \\ f(\tilde{z}) &= \tilde{z}/4 \quad \text{for} \quad \tilde{z} \ll 1 \quad (N \gg 1) \end{aligned} \qquad (4)$$

for thin and wide electron beam asymptote, respectively.

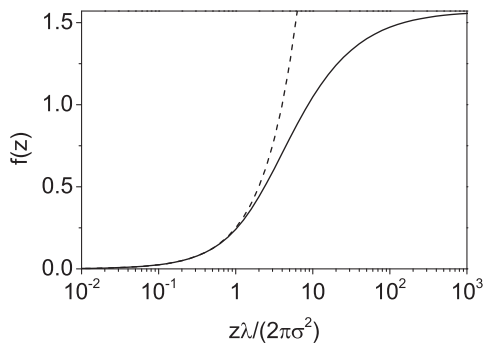

Figure 1: Function $f(z)$ entering equation (3). Dashed line shows the asymptote (4) for small values of z, $f(\tilde{z}) = \tilde{z}/4$.

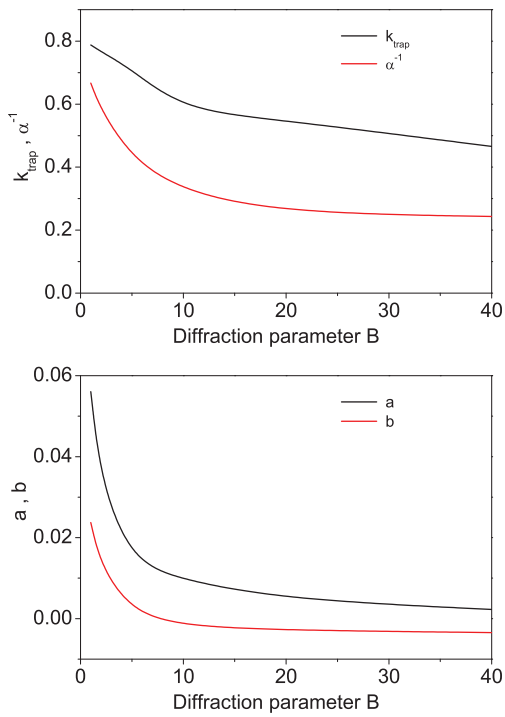

Figure 2: Upper plot: the trapping efficiency K_{trap} for the globally optimized undulator (black curve) and the fitting coefficient α_{tap}^{-1} of the global optimization entering Eq. (5) (red curve). Lower plot: coefficients a (black line) and b (red line) of the rational fit of the tapering law (6).

The detuning (undulator tapering) should follow the energy loss by particles given by (3) which suggests the following universal law [24, 25]:

$$\hat{C} = \alpha_{tap}(\hat{z} - \hat{z}_0)\left[\arctan\left(\frac{1}{2N}\right) + N\ln\left(\frac{4N^2}{4N^2+1}\right)\right]\,, \qquad (5)$$

with Fresnel number N fitted by $N = \beta_{tap}/(\hat{z} - \hat{z}_0)$. Undulator tapering starts by two field gain length $2 \times L_g$ before the saturation point at $z_0 = z_{sat} - 2 \times L_g$. Parameter β_{tap} is rather well approximated with the linear dependency on diffraction parameter, $\beta_{tap} = 8.5 \times B$. Parameter α_{tap} is

Copyright © 2015 CC-BY-3.0 and by the respective authors

ISBN 978-3-95450-134-2

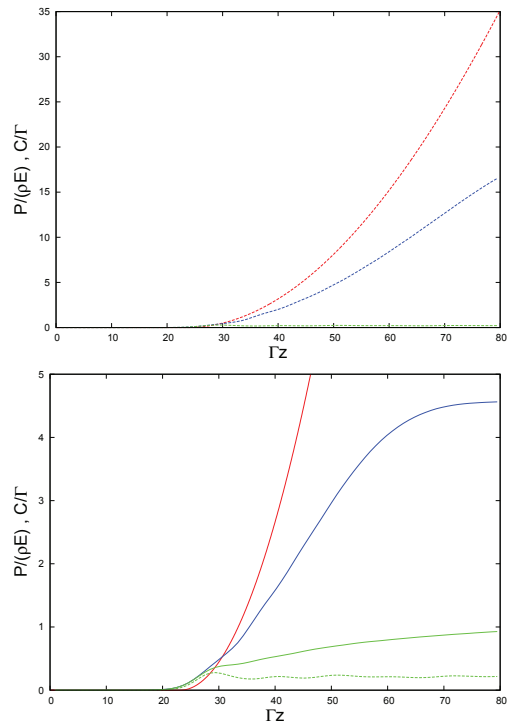

Figure 3: Evolution along the undulator of the reduced radiation power $\hat{\eta} = W/(\rho W_{\rm beam})$ (blue curve) and of the detuning parameter $\hat{C} = C/\Gamma$ (red curve). Top and bottom plots correspond to the seeded and SASE case, respectively. Solid blue and green curve on the bottom curve correspond to tapered and untapered case, respectively. Dashed green line is radiation power of seeded untapered FEL. Diffraction parameter is $B = 10$.

plotted in Fig. 2. It is a slow varying function of the diffraction parameter B, and scales approximately to $B^{1/3}$.

Analysis of the expression (5) shows that it has quadratic dependence in z for small values of z (limit of the wide electron beam), and linear dependence in z for large values of z (limit of the thin electron beam). It is natural to try a fit with a rational function which satisfies both asymptotes. The simplest rational fit is:

$$\hat{C} = \frac{a(\hat{z} - \hat{z}_0)^2}{1 + b(\hat{z} - \hat{z}_0)} \,. \qquad (6)$$

The coefficients a and b are the functions of the diffraction parameter B, and are plotted in Fig. 2. Start of the undulator tapering is set to the value $z_0 = z_{sat} - 2L_g$. Analysis performed in [24, 25] have shown that the fit of the tapering law with the rational function also works well.

ANALYSIS OF THE TAPERING PROCESS

Seeded FEL

We proceed our paper with the analysis of the trapping process. Top plot in Fig. 3 shows evolution of the average radiation power of seeded FEL along the optimized tapered undulator. The trapping efficiency $K_{trap} = \hat{P}/\hat{C}$ falls down with the diffraction parameter B (see Fig. 2). This is natural

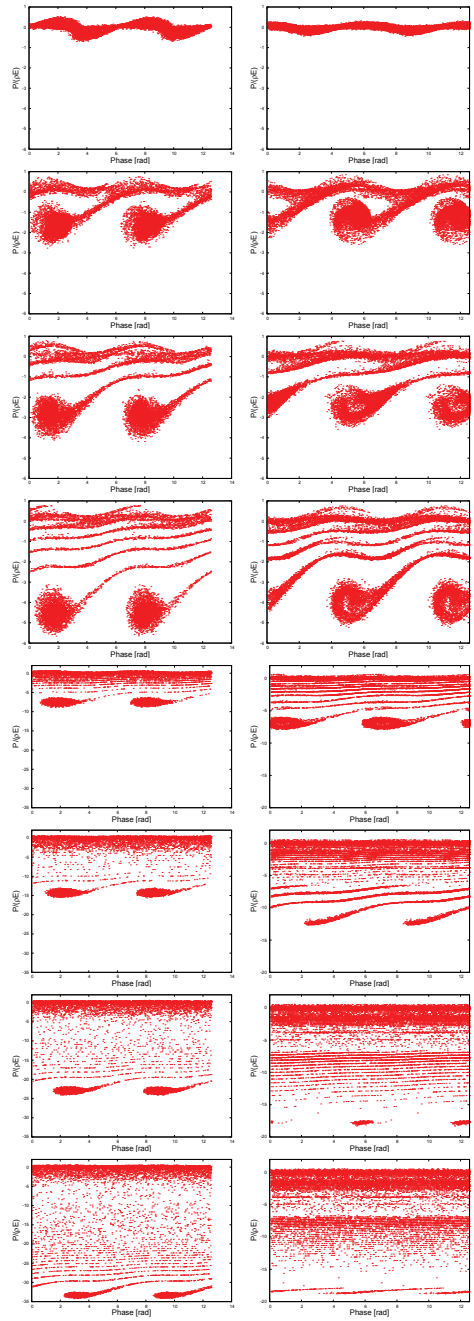

Figure 4: Phase space distribution of electrons at different stages of the trapping process. Diffraction parameter is $B = 10$. Plots from the top to the bottom correspond to $\hat{z} = 23.5$, 35.3, 39.2, 43.2, 49, 58.9, 68.7, and 78.5, respectively. Left column represents seeded FEL amplifier. Right column represents SASE FEL at the coordinate along the bunch $\hat{s} = \rho\omega t = 100$, see Figs. 5 and 6.

consequence of the diffraction effects discussed in earlier publications (see, e.g. Ref. [9], Chapter 4). Indeed, FEL radiation is not a plane wave. Transverse distribution of the radiation field (FEL radiation mode [9, 29]) depends on the value of the diffraction parameter B, and the field gradient (or, amplitude of ponderomotive well) across the electron

ISBN 978-3-95450-134-2

Copyright © 2015 CC-BY-3.0 and by the respective authors

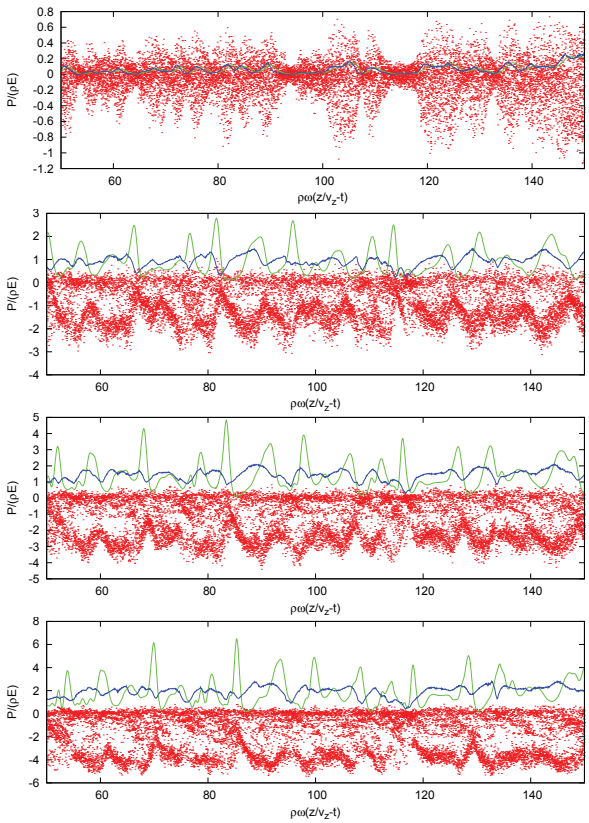

Figure 5: Phase space distribution of the particles along the bunch (red dots), average loss of the electron energy (blue line), and radiation power (green line) at different stages of the trapping process in SASE FEL. Here diffraction parameter is $B = 10$. Plots from the top to the bottom correspond to $\hat{z} = 23.5$, 35.3, 39.2, and 43.2, respectively.

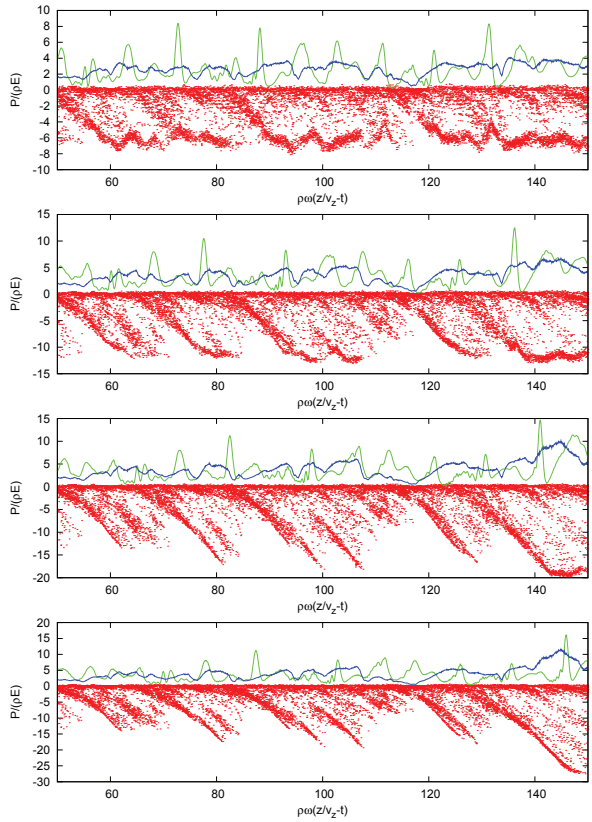

Figure 6: Phase space distribution of the particles along the bunch (red dots), average loss of the electron energy (blue line), and radiation power (green line) in the deep tapering regime. Diffraction parameter is $B = 10$. Plots from the top to the bottom correspond to $\hat{z} = 49$, 58.9, 68.7, and 78.5, respectively.

beam is more pronouncing for larger values of the diffraction parameter B. In the latter case we obtain situation when electrons located in the core of the electron beam are already fully bunched while electrons at the edge of the beam are not bunched yet (see phase space plot (a) in Fig. 4). As a result, the number of electrons with similar positions on the energy-phase plane falls down with the growth of the diffraction parameter, as well as the trapping efficiency in the regime of coherent deceleration. The trapping process is illustrated with the phase space plots presented on Figs. 4-6 for the value of the diffraction parameter $B = 10$. The particles in the core of the beam are trapped most effectively. Nearly all particles located at the edge of the electron beam leave the stability region very soon. The trapping process lasts for a several field gain lengths when the trapped particles become to be isolated in the trapped energy band for which the undulator tapering is optimized further. For the specific value of the diffraction parameter $B = 10$ the trapping proces is not finished even at three field gain lengths after saturation, and non-trapped particles continue to populate low energy tail of the energy distribution (see Fig. 7). There was an interesting experimental observation at LCLS that energy distribution of non-trapped particles is not uniform, but represent a kind of energy bands [30–32]. Graphs presented in Fig. 4 give a hint on the origin of energy bands which are formed by non-trapped particles. This is the consequence of nonlinear dynamics of electrons leaving the region of stability. Note that a similar effect can be seen in the early one-dimensional studies [7, 8].

Optimum Tapering of SASE FEL

The considerations on the strategy for the tapering optimization of a SASE FEL is rather straightforward. Radiation of SASE FEL consists of wavepackets (spikes). In the exponential regime of amplifications wavepackets interact strongly with the electron beam, and their group velocity visibly differs from the velocity of light. In this case the slippage of the radiation with respect to the electron beam is by several times less than kinematic slippage [9]. This feature is illustrated with the upper plot in Fig. 5 which shows onset of the nonlinear regime. We see that wavepackets are closely connected with the modulations of the electron beam current. When the amplification process enters nonlinear (tapering) stage, the group velocity of the wavepackets approaches to the velocity of light, and the relative slippage approaches to the kinematic one. When a wavepacket advances such that

Copyright © 2015 CC-BY-3.0 and by the respective authors

ISBN 978-3-95450-134-2

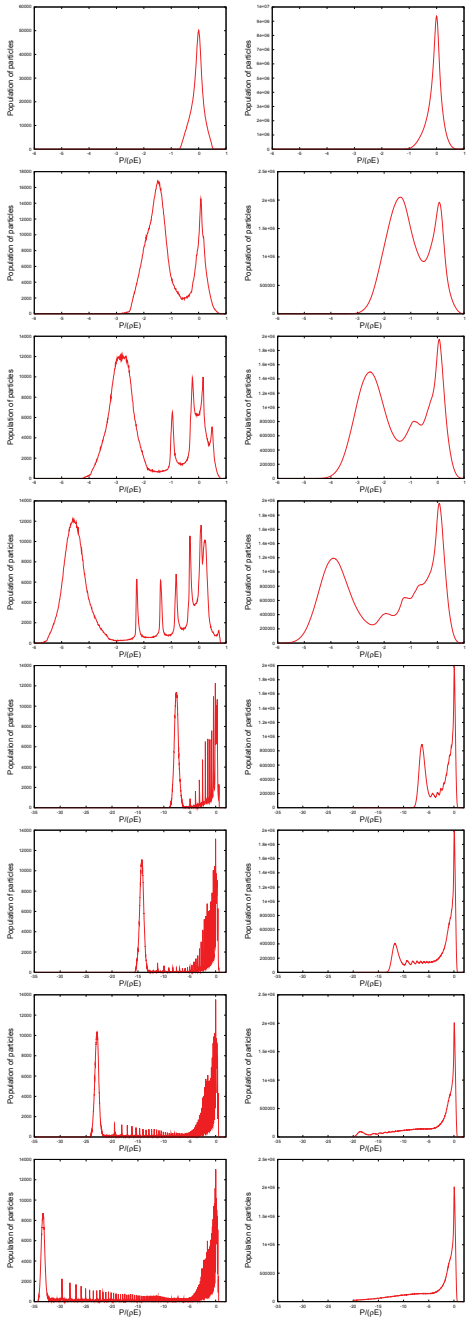

Figure 7: Population of the particles in energy at different stages of amplification. Diffraction parameter is $B = 10$. Plots from the top to the bottom correspond to $\hat{z} = 23.5$, 35.3, 39.2, 43.2, 49, 58.9, 68.7, and 78.5, respectively. Left and right columns represent seeded FEL amplifier and SASE FEL, respectively.

it reaches the next area of the beam disturbed by another wavepacket, we can easily predict that the trapping process will be destroyed, since the phases of the beam bunching and of the electromagnetic wave are uncorrelated in this case. Typical scale for the destruction of the tapering regime is coherence length, and the only physical mechanism we can use is to decrease the group velocity of wavepackets. This

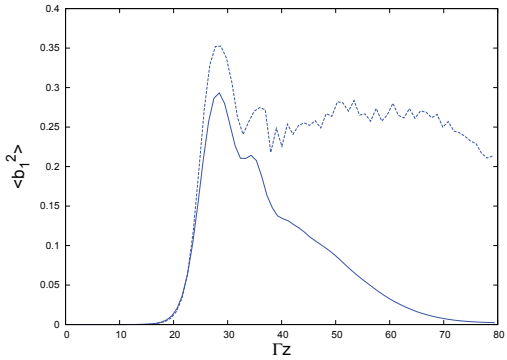

Figure 8: Evolution along the undulator of the squared value of the bunching factor for the FEL amplifier with optimized undulator tapering. Dashed and solid line represent seeded FEL amplifier and SASE FEL, respectively. Diffraction parameter is $B = 10$.

happens optimally when we trap maximum of the particles in the regime of coherent deceleration, and force these particles to interact as strong as possible with the electron beam. We see that this strategy is exactly the same as we used for optimization of seeded FEL. Global numerical optimization confirms these simple physical considerations. Conditions of the optimum tapering are the same as it has been described above for the seeded case. Start of the tapering is by two field gain lengths before the saturation. Parameter β_{tap} is the same, $8.5 \times B$. The only difference is the reduction of the parameter α_{tap} by 20% which is natural if one remember statistical nature of the wavepackets. As a result, optimum detuning is just 20% below the optimum seeded case.

We illustrate operation of SASE FEL with simulations with three-dimensional, time-dependent FEL simulation code FAST [33]. Bottom plot in Fig. 3 shows evolution of the average radiation power of SASE FEL along optimized tapered undulator. Details of the phase space distributions are traced with Figs. 4 - 6. Initially behavior of the process is pretty close to that of the seeded case. Initial values of the beam bunching is comparable with the seeded case (see Fig. 8). The rate of the energy growth is also comparable with the seeded case. The feature of the "energy bands" remains clearly visible in the case of SASE FEL as well (see Figs. 7 - 6). It is interesting observation that plots in Figs. 6 corresponding to the well trapped particles qualitatively correspond to experimental data from LCLS taken with transverse deflecting cavity [30–32].

The beam bunching gradually drop down when wavepackets travel along the bunch. As we expected, the amplification process is almost abruptly stopped when the relative slippage exceeded the coherence length. However, increase of the total radiation power with respect to the saturation power is about factor of 12.

ISBN 978-3-95450-134-2

Copyright © 2015 CC-BY-3.0 and by the respective authors

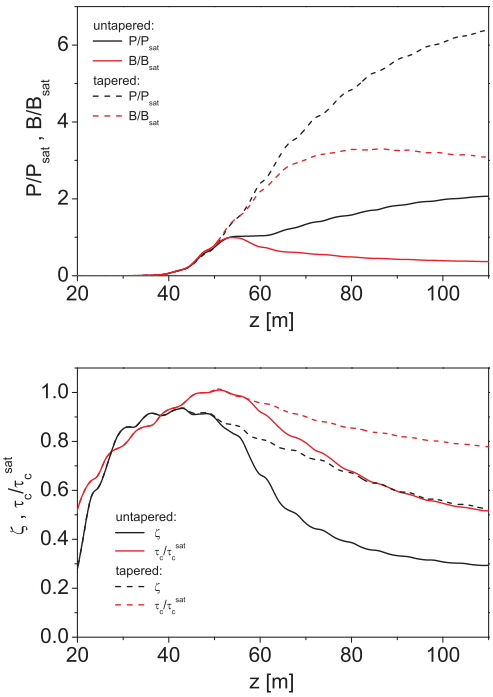

Figure 9: Fundamental harmonic: evolution of the radiation power and brilliance (top plot) and of coherence time and degree of transverse coherence (bottom plot) along the undulator for untapered (solid curves) and optimized tapered case (dashed curves).

PROPERTIES OF THE SASE RADIATION: TAPERED VERSUS UNTAPERED CASE

We perform comparative analysis of the radiation properties tapered and untapered case for the parameters of the SASE3 undulator of the European XFEL [34]. Undulator period is 6.8 cm, electron energy is 14 GeV, radiation wavelength is 1.55 nm. Undulator consists of 21 modules, each is 5 meters long with 1.1 m long intersections between modules. Parameters of the electron beam correspond to 0.25 nC case of the baseline parameters of the electron beam: emittance 0.6 mm-mrad, rms energy spread 2.5 MeV, peak beam current 5 kA [35]. Average focusing beta function is equal to 15 m. The value of the diffraction parameter is B = 1.1 which is close to the optimum conditions for reaching the maximum value of the degree of transverse coherence [36]. Two cases were simulated: untapered undulator, and the undulator optimized for maximum FEL efficiency as it has been described in previous sections [25].

Plots in Fig. 9 show evolution along the undulator of the radiation power, the degree of transverse coherence, the coherence time, and the brilliance for the fundamental harmonic. For the case of untapered undulator the coherence time and the degree of transverse coherence reach maximum values in the end of the linear regime. Maximum brilliance of the radiation is achieved in the very beginning of the nonlinear regime which is also referred as the saturation point [36]. In the case under study the saturation occurs at the undulator length of 53 m. Parameters of the radiation at the saturation point are: the radiation power is 108 GW, the coherence time is 1.2 fs, the degree of transverse coherence is 0.86, and the brilliance of the radiation is equal to 3.8×10^{22} photons/sec/mm^2/rad^2/0.1% bandwidth. The radiation characteristics plotted in Fig. 9 are normalized to the corresponding values at the saturation point.

General observations for the tapered regime are as follows. Radiation power grows faster than in the untapered tapered case. The coherence time and the degree of transverse coherence degrade, but a bit less intensive than in the untapered case. Brilliance of the radiation for the tapered case saturates at the undulator length of 80 m, and then drops down gradually. For this specific practical example the benefit of the tapered case against untapered case in terms of the radiation brilliance is factor of 3, and it is mainly defined by the corresponding increase of the radiation power. Coherence properties of the radiation in the point of the maximum brilliance of the tapered case are worse than those of the untapered SASE FEL in the saturation point: 0.86 to 0.68 for the degree of transverse coherence, and 1 to 0.86 in terms of the coherence time.

REFERENCES

[1] N.M. Kroll, P.L. Morton, and M.N. Rosenbluth, IEEE J. Quantum Electron. 17, 1436 (1981).

[2] T.J. Orzechowski, B.R. Anderson, J.C. Clark, e al., Phys. Rev. Lett. 57, 2172 (1986).

[3] R.A. Jong, E.T. Scharlemann, W.M. Fawley, Nucl. Instrum. Methods Phys. Res. A272, 99 (1988).

[4] W.M. Fawley, Nucl. Instrum. Methods Phys. Res. A375, 550 (1996).

[5] W.M. Fawley, Z. Huang, K.J. Kim, and N. Vinokurov, Nucl. Instrum. Methods Phys. Res. A483, 537 (2002).

[6] E.L. Saldin, E.A. Schneidmiller and M.V. Yurkov, Opt. Commun. 95, 141 (1993).

[7] E.T. Scharlemann, Laser Handbook, Volume 6, Free electron lasers, eds. W.B. Colson, C. Peilegrini and A. Renieri (North Holland, Amsterdam, 1991), p. 291.

[8] E.L. Saldin, E.A. Schneidmiller and M.V. Yurkov, Physics Reports 260, 187 (1995).

[9] E.L. Saldin, E.A. Schneidmiller, M.V. Yurkov, "The Physics of Free Electron Lasers" (Springer-Verlag, Berlin, 1999).

[10] E.L. Saldin, V.P. Sarantsev, E.A. Schneidmiller and M.V. Yurkov, Nucl. Instrum. and Methods A339. 583 (1994).

[11] C. Pagani, E.L. Saldin, E.A. Schneidmiller and M.V. Yurkov, Nucl. Instrum. and Methods A455, 733 (2000).

[12] E.A. Schneidmiller, V.F. Vogel, H. Weise and M.V. Yurkov, Journal of Micro/Nanolithogrphy, MEMS, and MOEMS 11(2), 021122 (2012).

[13] W. Ackermann, G. Asova, V. Ayvazyan et al., Nature Photonics 1, 336 (2007).

Copyright © 2015 CC-BY-3.0 and by the respective authors

ISBN 978-3-95450-134-2

[14] M. Vogt, B. Faatz, J. Feldhaus et al., Proc. IPAC 2014 Conf., paper TUOCA02 (2014), http://accelconf.web.cern.ch/AccelConf/IPAC2014/papers/tupca02.pdf

[15] E. Allaria, R. Appio, L. Badano et al., Nature Photonics 6, 699 (2012).

[16] P. Emma, R. Akre, J. Arthur et al., Nature Photonics 4, 641 (2010).

[17] Tetsuya Ishikawa, Hideki Aoyagi, Takao Asaka et al., Nature Photonics 6, 540 (2012).

[18] Massimo Altarelli, Reinhard Brinkmann, Majed Chergui et al. (Eds), XFEL: The European X-Ray Free-Electron Laser. Technical Design Report, Preprint DESY 2006-097, DESY, Hamburg, 2006 (see also http://xfel.desy.de).

[19] R. Ganter (Ed.), Swiss FEL Conceptual Design Report, PSI Bericht Nr. 10-04, April 2012.

[20] H.S. Kang, K.W. Kim, I.S. Ko, Proc. IPAC 2014 Conf., paper THPRO019 (2014), http://accelconf.web.cern.ch/AccelConf/IPAC2014/papers/thpro019.pdf

[21] X.J. Wang, H.P. Freund, D. Harder et al., Phys. Rev. Lett. 103, 154801 (2009).

[22] Y. Jiao, J. Wu, Y. Cai et al., Phys. Rev. ST Accel. Beams 15, 050704 (2012).

[23] G. Geloni, V. Kocharyan, and E. Saldin, DESY Report 11-049, 2011.

[24] E.A. Schneidmiller and M.V. Yurkov, Proc. FEL2014 Conference, Basel, Switzerland, 2014, MOP065. http://accelconf.web.cern.ch/AccelConf/FEL2014/papers/mop065.pdf

[25] E.A. Schneidmiller and M.V. Yurkov, Phys. Rev. ST Accel. Beams 18, 030705 (2015).

[26] E.L. Saldin, E.A. Schneidmiller and M.V. Yurkov, Nucl. Instrum. and Methods A 475, 86 (2001).

[27] R. Bonifacio, C. Pellegrini and L.M. Narducci, Opt. Commun. 50 (1984) 373.

[28] E.L. Saldin, E.A. Schneidmiller and M.V. Yurkov, Nucl. Instrum. and Methods A539, 499 (2005).

[29] E.T. Scharlemann, A.M. Sessler, and J.S. Wurtele, Nucl. Instrum. and Methods A 239, 29 (1985).

[30] C. Behrens, Talk at the Workshop on Advanced X-Ray FEL Development, May 23, 2014, Hamburg.

[31] P. Krejcik, Talk at IPAC 2014, June 2014, Dresden, Germany. http://accelconf.web.cern.ch/AccelConf/IPAC2014/talks/weobb03/talk.pdf

[32] Y. Ding, F.-J. Decker, V.A. Dolgashev et al., Preprint SLAC-PUB-16105, SLAC National Accelerator Laboratory, 2014.

[33] E.L. Saldin, E.A. Schneidmiller, and M.V. Yurkov, Nucl. Instrum. and Methods A 429, 233 (1999).

[34] E.A. Schneidmiller and M.V. Yurkov, J. Mod. Optics (2015). DOI: 10.1080/09500340.2015.1035349

[35] E.A. Schneidmiller and M.V. Yurkov, Preprint DESY 11-152, Hamburg, 2011.

[36] E.L. Saldin, E.A. Schneidmiller, and M.V. Yurkov, Opt. Commun. 281(2008)1179.

Copyright © 2015 CC-BY-3.0 and by the respective authors

ISBN 978-3-95450-134-2